

RESEARCH ARTICLE

Interfacial mechanisms for stability of surfactant-laden films

M. Saad Bhamla^{1*}, Chew Chai², Marco A. Álvarez-Valenzuela³, Javier Tajuelo⁴, Gerald G. Fuller²

1 Stanford University, Department of Bioengineering, Stanford, 94305, United States of America, **2** Stanford University, Department of Chemical Engineering, Stanford, 94305, United States of America, **3** Universidad Carlos III de Madrid, Department of Mechanical Engineering, Leganes, 28911, Spain, **4** Universidad Nacional de Educación a Distancia (UNED), Departamento de Física Fundamental, Madrid, 28040, Spain

* saadbhamla@gmail.com



Abstract

Thin liquid films are central to everyday life. They are ubiquitous in modern technology (pharmaceuticals, coatings), consumer products (foams, emulsions) and also serve vital biological functions (tear film of the eye, pulmonary surfactants in the lung). A common feature in all these examples is the presence of surface-active molecules at the air-liquid interface. Though they form only molecular-thin layers, these surfactants produce complex surface stresses on the free surface, which have important consequences for the dynamics and stability of the underlying thin liquid film. Here we conduct simple thinning experiments to explore the fundamental mechanisms that allow the surfactant molecules to slow the gravity-driven drainage of the underlying film. We present a simple model that works for both soluble and insoluble surfactant systems in the limit of negligible adsorption-desorption dynamics. We show that surfactants with finite surface rheology influence bulk flow through viscoelastic interfacial stresses, while surfactants with inviscid surfaces achieve stability through opposing surface-tension induced Marangoni flows.

OPEN ACCESS

Citation: Bhamla MS, Chai C, Álvarez-Valenzuela MA, Tajuelo J, Fuller GG (2017) Interfacial mechanisms for stability of surfactant-laden films. PLoS ONE 12(5): e0175753. <https://doi.org/10.1371/journal.pone.0175753>

Editor: Jay D. Schieber, Illinois Institute of Technology, UNITED STATES

Received: November 8, 2016

Accepted: March 30, 2017

Published: May 17, 2017

Copyright: © 2017 Bhamla et al. This is an open access article distributed under the terms of the [Creative Commons Attribution License](https://creativecommons.org/licenses/by/4.0/), which permits unrestricted use, distribution, and reproduction in any medium, provided the original author and source are credited.

Data Availability Statement: Individual data-sets for all experiments are available through FigShare: <https://doi.org/10.6084/m9.figshare.c.3736687.v1>.

Funding: The authors received no specific funding for this work. However, J. T. acknowledges a personal grant from UNED's Researchers Formation Program and partial support from MINECO (Grant FIS2013-47350-C5-5-R).

Competing interests: The authors have declared that no competing interests exist.

Introduction

Stability and drainage of thin surfactant films is relevant across various disciplines: industrial applications including engineered foams and emulsions [1], fundamental physics of bubbles [2–4], bio-foams in aquatic animal nests [5], and physiological systems including the human tear film [6] and pulmonary surfactants [7]. However, the drainage rate of these thin films depends critically on the mechanism through which these films are stabilized, which in turn is strongly coupled to the chemical composition of the surfactants.

The majority of past literature has looked at the stability of thin films in presence of soluble amphiphiles, including drainage from horizontal films [8, 9], drainage of vertical films based on Frankel's law [10, 11] and film stability in fiber coating experiments [12]. In comparison, the problem of drainage in presence of insoluble surfactants has been studied relatively less due to experimental challenges; the majority of investigations by Naire and coworkers focused on mathematical models to study the drainage of vertical thin films in the presence of insoluble

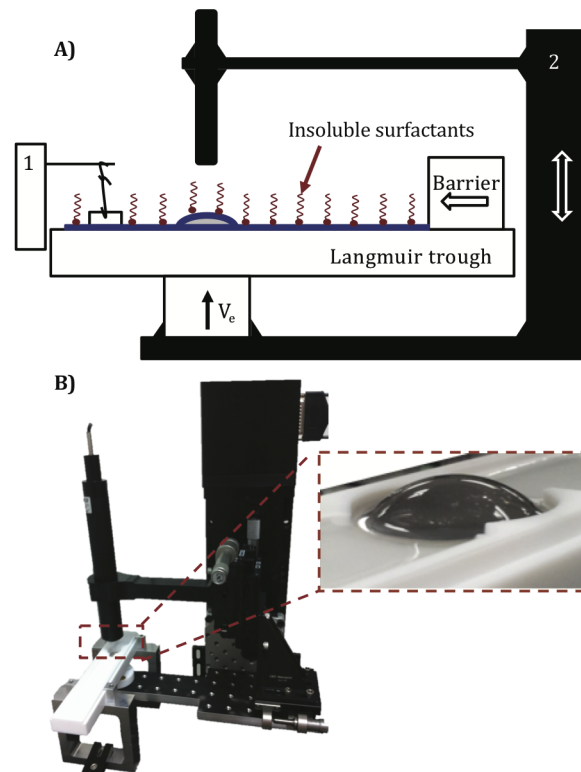


Fig 1. Experimental platform. Schematic (A) and photograph (B) of the drainage platform. For the insoluble surfactant experiments, the glass dome is initially submerged in the PBS-filled Langmuir trough (white, teflon container) and DPPC is spread at the air-liquid interface. DPPC is then compressed to the desired surface pressure using a single Delrin barrier and the surface pressure is monitored using a paper Wilhelmy balance (1). For the soluble surfactant experiments, the Langmuir trough is filled with SDS solution of desired concentration. In both cases, the measurement commences once the glass dome is elevated through air-liquid interface with a computer controlled motorized stage (2). A high speed interferometer (black tube) captures the thickness of the draining films as a function of time at the apex of glass dome.

<https://doi.org/10.1371/journal.pone.0175753.g001>

surfactants [13–15]. Past work by Joye et al. also presents numerical simulations and linear stability analysis to explore the role of surface rheological parameters [16, 17]. However, there is a need for a simple experimental platform that can systematically compare both soluble and insoluble surfactants, with varying surface rheologies and quantify the drainage dynamics using a simple theoretical model.

Here we utilize a simple setup (Fig 1) to measure the drainage dynamics of surfactant-laden aqueous films. Thin films of liquid are created by elevating an initially submerged curved glass substrate through the air-liquid interface at controlled velocities (V_e). A high-speed interferometer enables measurement of the varying film thickness at the apex of the film. We employ two heavily-studied commercial surfactants: 1, 2-dipalmitoyl phosphatidylcholine (DPPC), an insoluble surfactant that forms viscoelastic interfaces [18, 19] and sodium dodecyl sulfate (SDS), a soluble surfactant that forms inviscid interfaces [20]. We also show by surface flow visualization that the viscoelasticity of DPPC films resists surface deformation and creates an *immobile* interface at high surface pressures, while the SDS films are more fluid-like and yield extremely mobile interfaces. The remarkably different surface properties between DPPC and SDS allow us to systematically explore the role of surface mobility on drainage dynamics.

Results and discussion

Theoretical hydrodynamic model for draining films with complex interfaces

Consider a hemispherical glass dome that is raised through a bulk of liquid that results in the capture of a thinning liquid film with a complex surfactant-laden interface. Deformation of the interface leads to interfacial stresses that need to be accounted for in the hydrodynamic model capturing the evolution of this thin film. Analytical solution to this thin-film draining problem is well-established in our past work [6, 7]. Briefly, the draining film behaves as a lubricating film that thins under the driving influence of gravitational stresses, with a no-slip boundary condition on one side (liquid-dome), and a tangential interfacial stress boundary condition on the other (liquid-air). To account for the surfactants at the air-liquid interface, we use the Boussinesq-Scriven model for the interface, which characterizes the surfactant layer with a surface tension (σ), surface shear viscosity (η_s), and surface dilatational viscosity (η_d). A key assumption to note is that we assume that surfactant transport is convection-dominated (surface Peclet number, $Pe_s \gg 1$), and thus neglect the adsorption-desorption dynamics for surfactants in our model.

From this mathematical analysis, the following single-parameter expression predicts the dimensionless thickness H of the film at the apex, due to gravity, as a function of time:

$$H = \frac{h}{h_0} = \frac{1}{\sqrt{1 + 4\alpha\tau}}, \quad (1)$$

where $\tau = t\rho gh_0^2/(\eta R)$ is the dimensionless time normalized by known experimental variables: bulk viscosity (η), substrate curvature (R), density (ρ), gravitational constant (g), time (t) and initial film thickness (h_0). The parameter α serves as a fitting-parameter that characterizes the fluidity of the interface and is directly coupled to the total Boussinesq number, $Bq = Bq_s + Bq_d + Ma$, where Bq_s , Bq_d and Ma are dimensionless numbers capturing the influence of surface shear viscosity, surface dilatational viscosity and Marangoni stresses. These numbers are defined as follows: $Bq_s = \eta_s/(\eta h_0)$, $Bq_d = \eta_d/(\eta h_0)$ and $Ma = R^2/(\rho gh_0^3)\nabla_s\sigma$, where η_s , η_d are the surface shear and dilatational viscosity due to the surfactant-molecules, ∇_s is the in-plane surface gradient at the air-liquid interface [7]. The total Boussinesq number captures the relative drag from the interface to the bulk due to combined influence of shear, dilatational and Marangoni stresses.

At the asymptotic limits of this model, the parameter α has exact analytical values: $\alpha = 1/3$ when $Bq = 0$ (surfactant-free interface), and $\alpha = 1/12$ for $Bq \rightarrow \infty$ (extremely viscous surfactant-laden interface) [6]. Using both numerical simulations and experiments, we have found that α transitions strongly at $Bq = 1$ [6]. This model has been shown to work well with commercial lung surfactant systems that contained a mixture of unknown soluble and insoluble components [7]. The purpose of this paper is to employ commonly-used systems that can be systematically controlled to provide conclusive evidence of stabilizing interfacial mechanisms. The parameter α , thus allows us to evaluate the role of interfacial contributions, including surface viscosities (Bq_s , Bq_d) and surface-tension gradients (Ma) on the draining behavior of thin films. However, by itself, α is insufficient to inform the relative contributions of surface rheology versus Marangoni effects. Thus, we further conduct surface flow visualization experiments that help in distinguishing between these different interfacial phenomena.

Insoluble surfactant: DPPC

For insoluble surfactants, it is common to connect the surface concentration through the surface pressure $\Pi = \gamma_0 - \gamma$, where γ and γ_0 are the surface tension with and without surfactants, respectively. For DPPC films, increasing the surface pressure has the effect of increasing both the surface shear and dilatational moduli [19, 21–23]. We conduct a surface pressure sweep from $\Pi = 5$ – 25 mN m^{-1} i.e., from the liquid-expanded (LE) phase to the liquid-condensed (LC) phase for DPPC, and measure the drainage of the films. A characteristic drainage experiment data-set is shown in Fig 2, revealing a good-fit of our model to the experimental data.

We further present data for $\Pi = 5$ and 25 mN m^{-1} in Fig 3A and 3B. In these figures, the inverse-squared film thickness $1/H^2 = (h_0/h)^2$ is plotted as a function of τ , for different films raised at varying elevation velocities, $V_e = 1$ – 10 mm s^{-1} . At both surface pressures, $\Pi = 5$ and 25 mN m^{-1} , the data trends linearly, yielding extremely good fits to our simple drainage model. Using Eq 1, the corresponding α values are shown in Fig 3C, for the span of surface pressures examined.

At higher surface pressures ($\Pi > 10 \text{ mN m}^{-1}$), $\alpha = 0.1$ is in good agreement to the theoretical prediction for a no-slip interfacial boundary condition ($\alpha = 0.08$, $Bq \rightarrow \infty$) and expected for DPPC due to its finite surface viscoelastic properties ($Bq_s, Bq_d \gg Ma$) [21, 22]. It is worth noting that the surface rheology of DPPC is dominated by its viscous modulus, even at high surface pressures, thus we can neglect the effect of surface elasticity [6]. In the absence of surfactants, the films should drain rapidly ($Bq = 0$) and have no added interfacial stabilization mechanism. We observe this for pure water films as they drain almost instantly ($< 50 \text{ ms}$), and cannot be captured using our interferometric technique. It is important to note that for DPPC, the dilatational viscosity is three orders of magnitude larger than its shear counterpart, and thus may play a more dominant role in stabilization ($Bq_d > Bq_s$) [22]. However, at lower surface pressures ($\Pi < 10 \text{ mN m}^{-1}$), DPPC has a more fluid-like interface, and obtaining the same value of $\alpha = 0.1$ hints that perhaps Marangoni stresses play a significant role in stabilization. We reinforce this observation by specifically conducting drainage experiments within the LE-LC plateau ($\Pi = 7 \text{ mN m}^{-1}$), where both the shear and dilatational moduli are negligible, and obtain a consistent value of $\alpha = 0.11$ (Fig 2). Moreover, the α values also show slightly

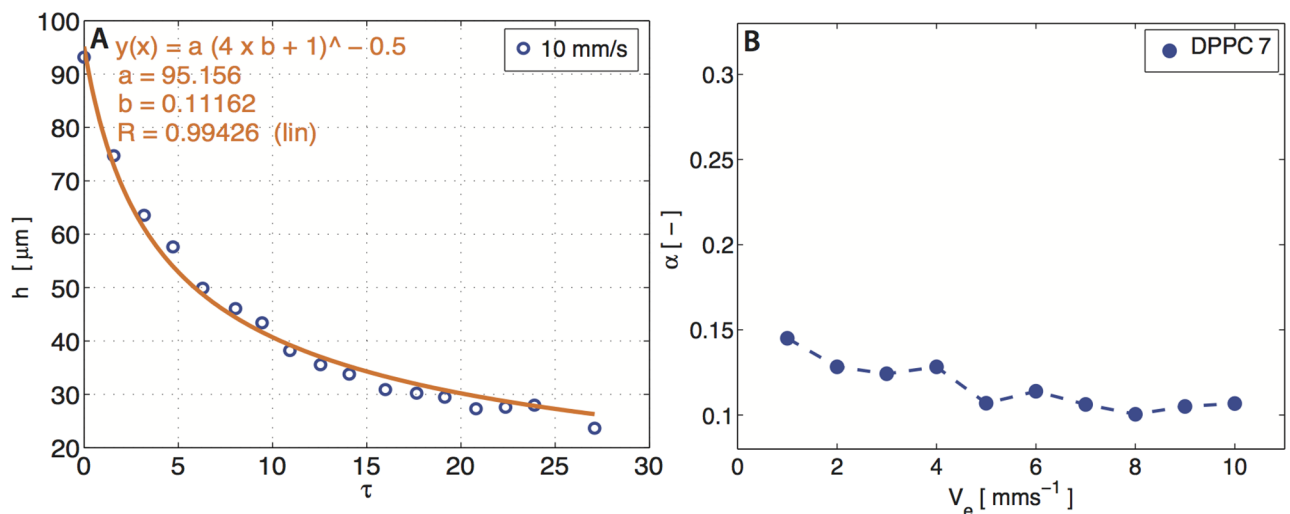


Fig 2. Characteristic experimental data-set for DPPC film drainage at 7 mN m^{-1} in the LE-LC plateau. (A) The film thickness (h) as a function of rescaled time (τ) at elevated $V_e = 10 \text{ mm s}^{-1}$. The parameter b corresponds to fitting parameter α . (B) Summary of the α values as a function of elevation velocity $V_e = [1$ – $10] \text{ mm s}^{-1}$.

<https://doi.org/10.1371/journal.pone.0175753.g002>

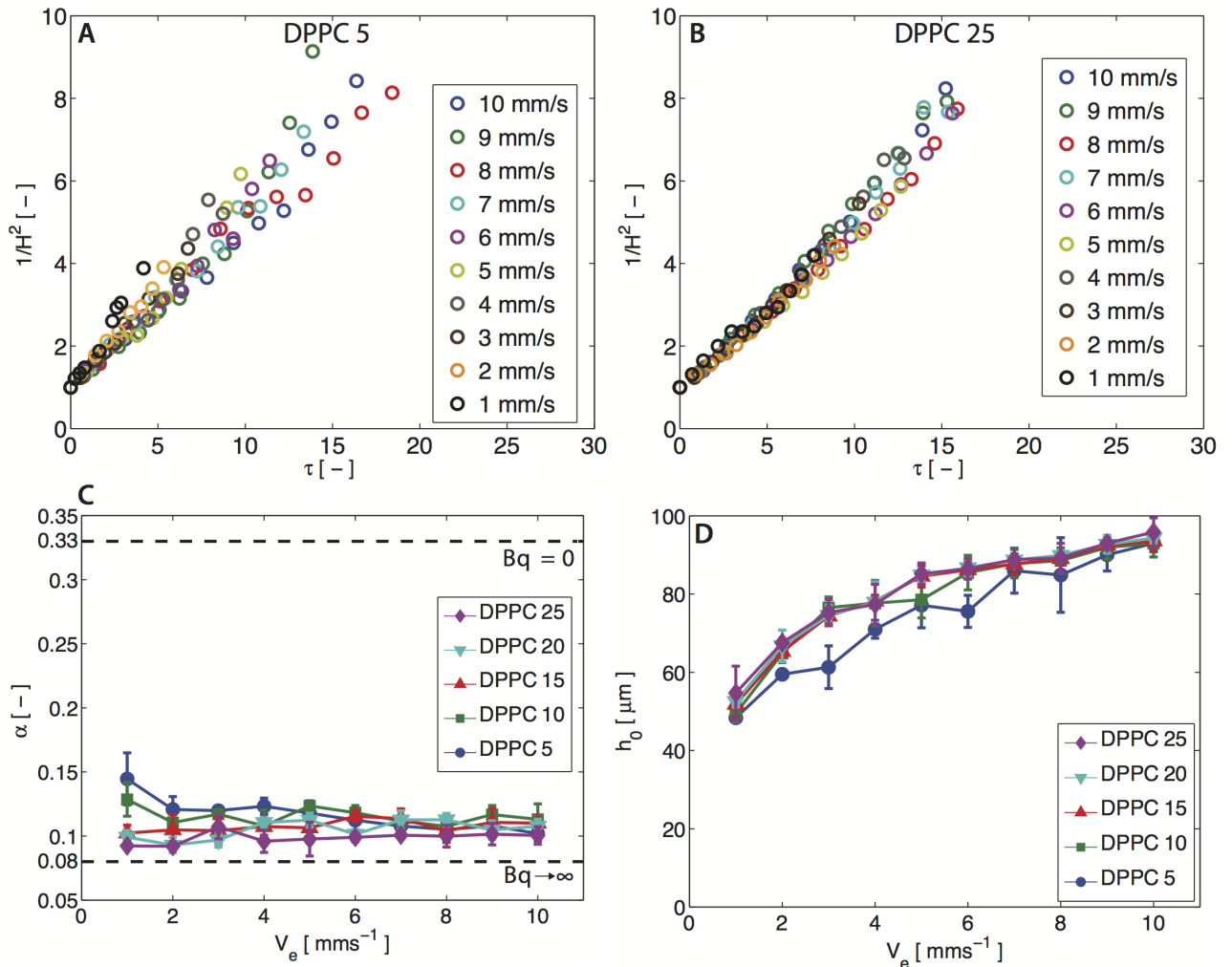


Fig 3. DPPC drainage experiments. (A, B) Dimensionless variable ($1/H^2 = (h_0/h)^2$) as a function of rescaled time (τ) for DPPC at 5 mN m^{-1} and 25 mN m^{-1} at various elevated velocity (V_e) ranging from 1–10 mm s^{-1} . (C) Summary of the value for the fitting parameter α of DPPC at various surface pressures. (D) Summary of the initial height capture of the aqueous film laden with DPPC at different surface pressures. The standard deviation is calculated from three independent trials.

<https://doi.org/10.1371/journal.pone.0175753.g003>

larger variations (0.09–0.15) at these low surface pressures. We will later demonstrate that Marangoni effects become important for DPPC films at low surface pressures ($Ma > Bq_s, Bq_d$), using surface flow visualization experiments.

We also report the initial height h_0 of the DPPC-laden films as a function of elevation velocity (V_e) in Fig 3D. We find that increasing the elevation speed results in the capture of thicker DPPC-laden films. This is expected due to the increased lubrication pressure in the thin film ($h \sim R\sqrt{Ca}$), where Ca is the Capillary number defined as $Ca = \eta V_e / \gamma$ [24]. Thus, the faster the elevation velocity, the thicker the film that is captured.

Soluble surfactant (SDS)

For SDS films, elevation velocity sweeps ($V_e = 1\text{--}10 \text{ mm s}^{-1}$) are conducted for two concentrations, below and above the cmc. We again plot the inverse-squared film thickness $1/H^2$ as a

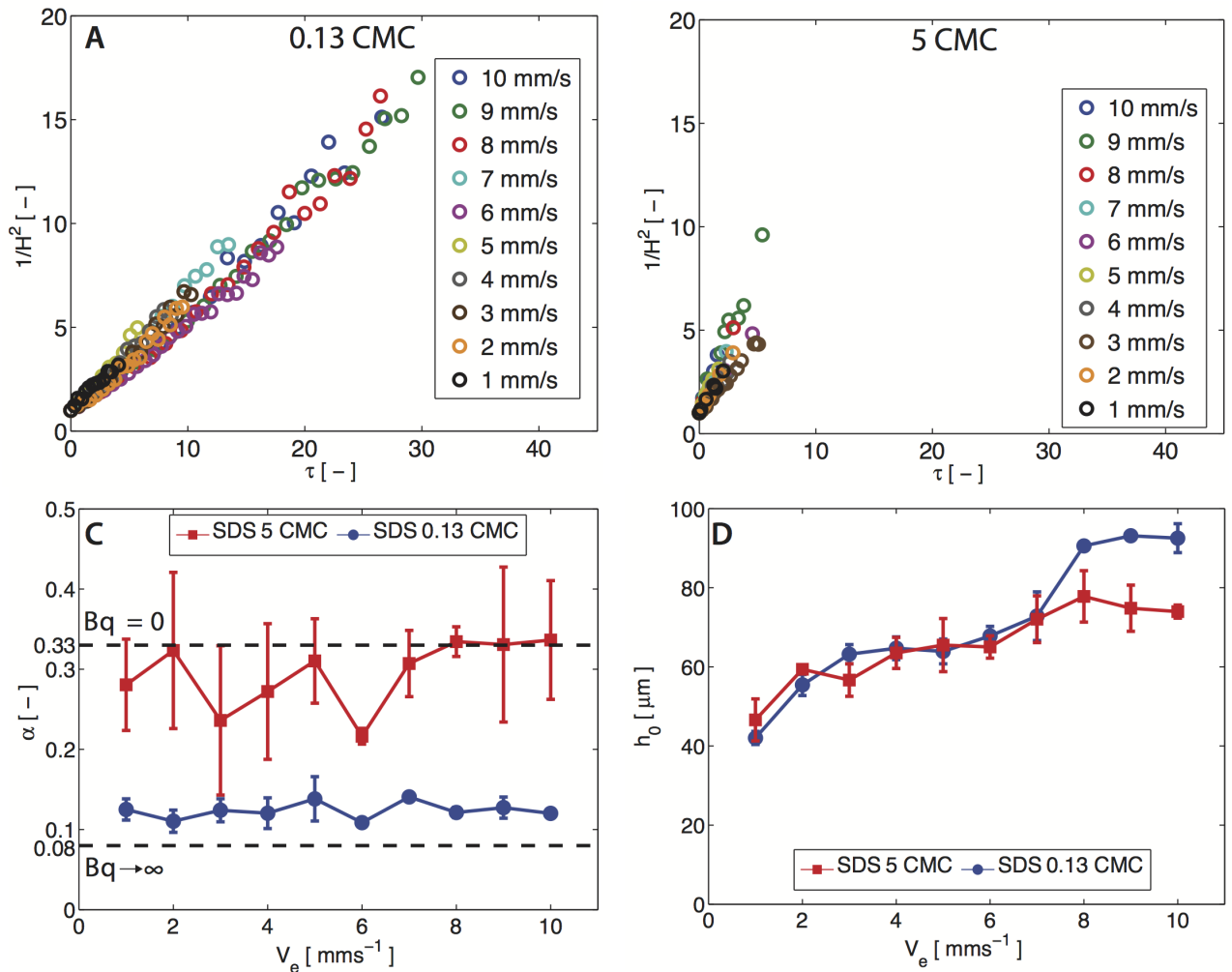


Fig 4. SDS drainage experiments. [A, B] Dimensionless variable ($1/H^2 = (h_0/h)^2$) as a function of rescaled time (τ) for SDS at 0.13 cmc and 5 cmc at various elevated velocity (V_e) ranging from 1–10 mm s⁻¹. [C] Summary of the value for the fitting parameter α of SDS at 0.13 cmc and 5 cmc. [D] Summary of the initial height capture of SDS film at 0.13 cmc and 5 cmc. The standard deviation is calculated from two independent trials.

<https://doi.org/10.1371/journal.pone.0175753.g004>

function of τ for films elevated at different V_e in Fig 4(A) and 4(B). For both cases, above and below cmc, the data again exhibits linear trends. However for the above cmc case, the SDS films drain extremely rapidly, and only a few data-points can be recorded, and we discuss the physical reason for this rapid-thinning below. In both cases, the data fits well to our simple model (S1 Fig), and the corresponding α values for SDS are shown in Fig 4C.

For SDS below its cmc, we obtain $\alpha \sim 0.10$ which is similar to α 's obtained for DPPC films. Thus, SDS and DPPC both stabilize against film drainage. However, it is well-established that SDS films have inviscid surfaces [20], ruling out the role of surface rheology ($Bq_s, Bq_d = 0$). Thus, this stabilization has to occur via strong surface-tension gradients or Marangoni flows ($Ma > 0$), which will indeed be confirmed using surface flow visualization in the next section.

Above the cmc, SDS films are less stable and drain rapidly with $\alpha \sim 0.3$. These drainage rates have significant error bars as the films drain almost instantly and only a few data-points can be recorded—the duration of drainage is < 2 s (see S1 Fig). We also note that above the

cmc, the adsorption time-scales are significantly shorter (~ 0.01 s, see SI) than the duration of drainage (S1 Fig), indicating that interfacial dynamics are governed by adsorption rather than convection at this concentration. Since our theoretical model does not include adsorption-desorption dynamics, the α values should be treated with caution for SDS above the cmc. Below the cmc, the interfacial dynamics are convection-dominated, since adsorption time scales are longer (>10 s, see SI) than the drainage times scales. Thus, $\alpha \sim 0.10$ values from our model accurately capture the role of Marangoni flows in stabilization of the SDS films below cmc.

Finally, we also show the initial entrained height (h_0) of the SDS films as a function of V_e in Fig 4D. At both concentrations, faster elevation velocities lead to larger initial thicknesses, similar to our observation for DPPC films, due to increased lubrication pressures. We also observe that for $V_e > 6 \text{ mm s}^{-1}$, films above the cmc concentration are relatively thinner than solutions below the cmc. Similar decreases in thickness have been observed in SDS entrainment experiments on fibers and are a consequence of micellar kinetics that reduces the Marangoni-induced stress, resulting in thinner films [12, 25, 26].

Surface flow visualization

In order to access the dominating influences of surface rheology (Bq_s, Bq_d) vs. Marangoni stresses (Ma) for DPPC and SDS films, we substitute the glass dome by an air bubble (Fig 5). The air bubble provides an enhanced refractive index contrast, resulting in extremely vibrant thin-film color interference patterns under white-light illumination. These color fringes vary in space and time, revealing the surface flows or lack thereof, and can be seen clearly in the attached supplementary movie files (S1–S4 Videos). Compiled time snapshots of DPPC and SDS are shown in Figs 6 and 7, respectively. It is useful to use the previously defined terminology for similar surface flows observed using a Scheludko-Exerowa setup by Joye et al. [16] These authors categorize the patterns as: *symmetric*, associated with surfaces possessing large surface shear and dilatational viscoelasticities; and *asymmetric*, associated with surfaces with low surface rheology, that yield to surface-tension induced Marangoni flows.

For DPPC, both the symmetric and asymmetric drainage patterns can be observed, as its surface rheology is a strong function of surface pressure. At low surface pressures ($\Pi = 5 \text{ mN m}^{-1}$), the DPPC film is initially symmetric, with circular fringe patterns ($t < 2$ s). However, this stable pattern is quickly deformed by plumes of surfactant rising from the periphery. These surface flows are fundamentally similar to rising plumes in vertical soap films, commonly referred to as ‘marginal regeneration’ [27–31]. These plumes are driven by surface-tension gradients and can be explained as follows. The dilation of the air-liquid interface creates a new surface area, resulting in a lower density of the surfactant near the apex. This creates a local area of high surface tension which pulls liquid from the bulk liquid (periphery) that is at a lower surface tension as illustrated in Fig 8. This results in rising plumes from the periphery towards the apex that re-distribute the DPPC molecules, resulting in a heterogeneous pattern that slowly thins, and ultimately the film bursts at $t \sim 10$ s.

At higher surface pressures $\Pi > 25 \text{ mN m}^{-1}$, DPPC films exhibit significant surface viscoelasticity, which suppresses all Marangoni flows. We thus observe stable and symmetric patterns that persist over the entire duration of drainage $t = 30$ s, until the film bursts. Similar stable patterns have also been observed for other viscoelastic lipids [7]. This reinforces our observation that for DPPC films, increasing the surface pressure transitions the stabilization mode from a Marangoni-dominated at low pressures to viscoelasticity-dominated at higher surface pressures.

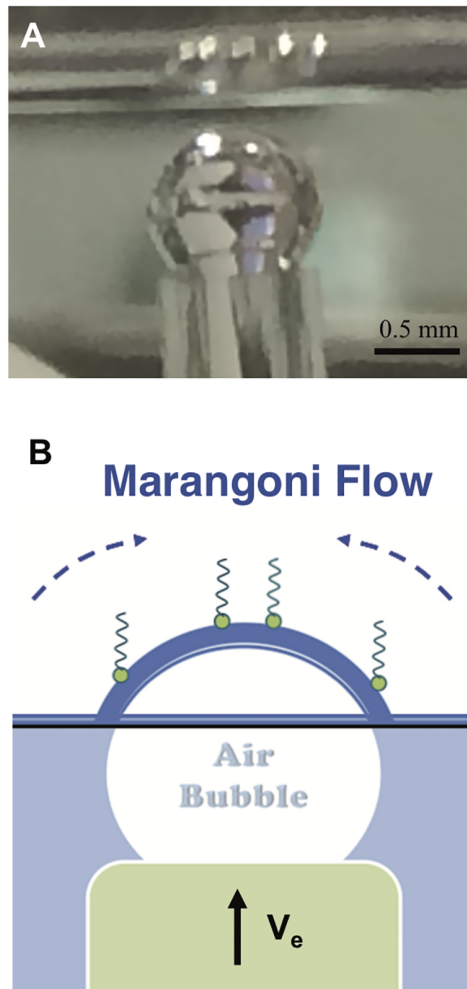


Fig 5. Surface flow visualization. Photograph (A) and schematic (B) of the surface visualization setup. Instead of a glass substrate, an air bubble is elevated through air-water interface. Thin film color interference patterns are clearly visible under diffused white-light illumination, due to enhanced refractive index mis-match.

<https://doi.org/10.1371/journal.pone.0175753.g005>

SDS films at 0.13 cmc and 5 cmc do not possess any measurable surface rheology [20]. Thus, we would expect these films to exhibit asymmetric drainage, dominated by Marangoni flows. From Fig 7 for SDS below cmc, we observe the rising plumes from the periphery towards the apex driven by surface-tension gradients. These ultimately lead to stabilization of the draining bulk film similar to that of DPPC at low surface pressures. Now, based on our drainage data discussed in Fig 4, we would expect the above cmc films to drain faster due to competing adsorption dynamics; however, the surface visualization data in Fig 7 shows otherwise. We actually observe strong Marangoni flows that act to stabilize the film significantly. This is due to the fact that we have extremely thin films in the bubbles ($< 1\mu\text{m}$) in comparison to the thicker films that the solid dome captures ($\sim 100\mu\text{m}$). It is well-established that in the thinner films, the adsorption times are longer than previously discussed, which ultimately lead to stronger Marangoni flows [32]. It is worth noting that for the solutions above the cmc, we also observe formation of black films before rupture. Thus, as quantitatively described in our drainage experiments, SDS films above and below cmc stabilize via Marangoni stresses, as the surfaces do not possess any surface viscoelasticity to quench these flows.

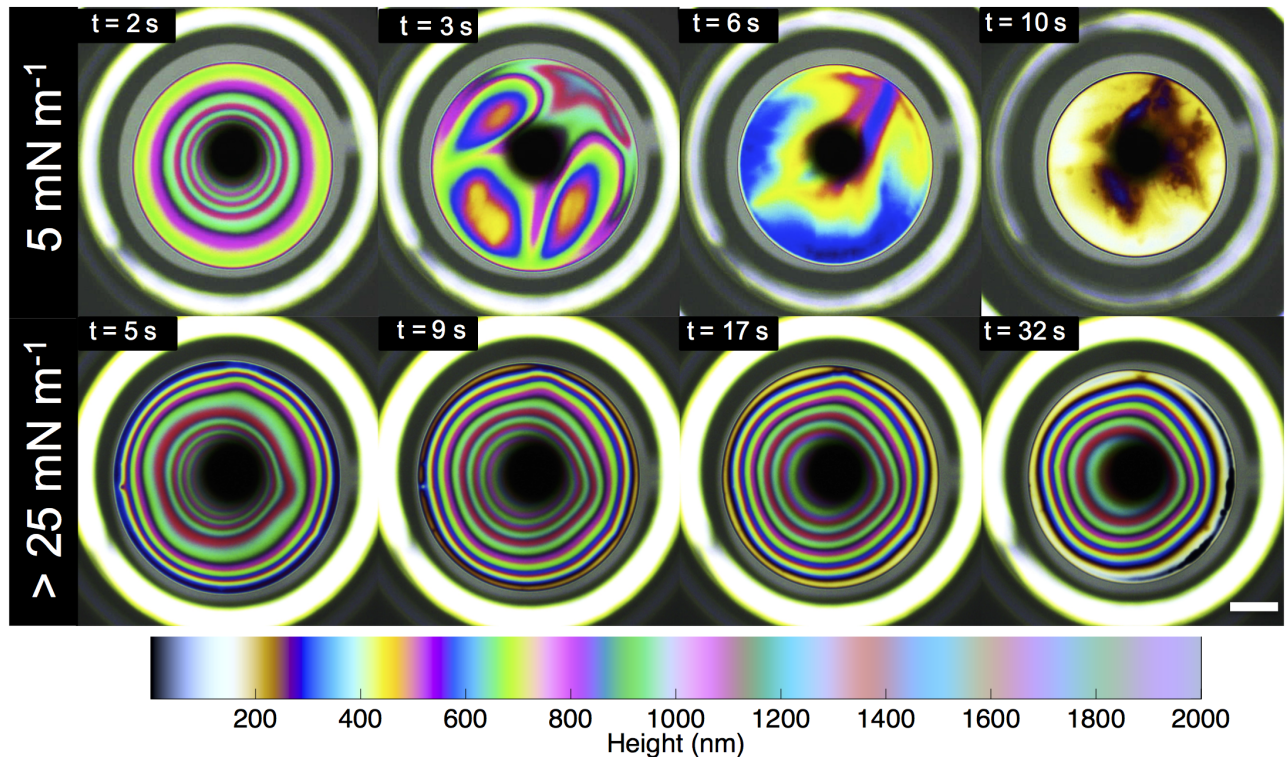


Fig 6. DPPC surface visualization. Images of the color interference patterns captured for DPPC at two different surface pressures, $\Pi = 5 \text{ mN m}^{-1}$ and $>25 \text{ mN m}^{-1}$ using the surface flow visualization setup. The colormap is a visual tool to determine the corresponding thickness of individual vibrant color. The dark black spot in the center of each frame is the reflection of the camera and the white bright ring at the periphery is the edge of the glass capillary. The scale bar shown is 0.25 mm.

<https://doi.org/10.1371/journal.pone.0175753.g006>

Conclusion

It is common knowledge that the presence of surfactants (e.g. soap) extend the life span of thin films (e.g. bubbles). However, a systematic comparison between the drainage of soluble and insoluble surfactants has not been previously presented. We offer an experimental platform to measure the gravity-driven drainage dynamics of DPPC (insoluble) and SDS (soluble) films, as well as a simple model that can be employed to evaluate the influence of interfacial phenomena in the absence of adsorption dynamics. We show that the presence of both DPPC and SDS at the air-liquid interface increases the stability of thin films. Specifically, DPPC films are stabilized through interfacial rheology at high surface pressures, resulting in immobile surfaces and Marangoni stresses at low surface pressures, resulting in mobile surfaces. Thus, the surface pressure of DPPC serves as a control for switching surface mobility on and off. Finally, SDS films are stabilized purely through Marangoni effects, resulting in mobile surfaces both above and below cmc. We thus show that soluble and insoluble surfactant systems exploit two fundamentally unique interfacial mechanisms to achieve the same result: thin film stability.

Materials and methods

Surfactants

Two commercially available surfactants are compared: 1, 2-dipalmitoyl phosphatidylcholine (DPPC) and sodium dodecyl sulfate (SDS). DPPC is purchased from Avanti Polar Lipids Inc.

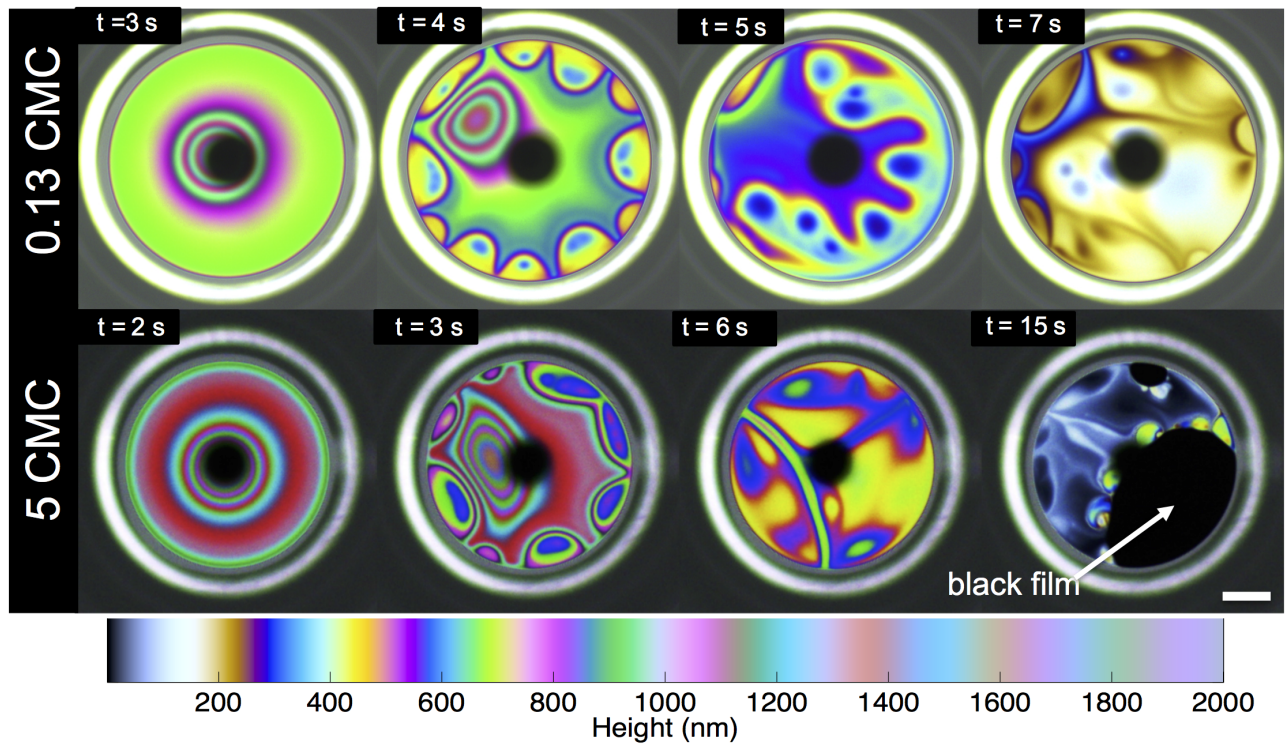


Fig 7. SDS surface visualization. Snapshots of interference patterns observed for SDS at 0.13 cmc and 5 cmc. The images are attained using the surface flow visualization setup. The colormap is a guide to relate individual vibrant color to its corresponding thickness. The dark black spot in the center of each frame is the reflection of the camera and the white bright ring at the periphery is the edge of the glass capillary. The scale bar shown is 0.25 mm.

<https://doi.org/10.1371/journal.pone.0175753.g007>

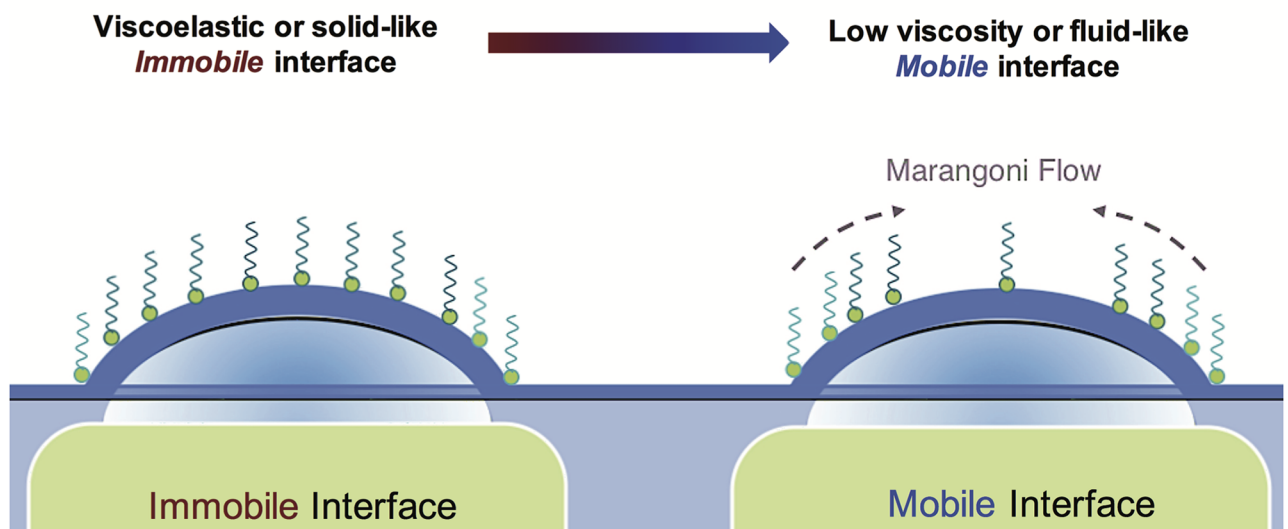


Fig 8. Surfactant stability mechanisms. Schematic summarizing the two different stabilizing interfacial mechanisms for surfactant films: Viscoelastic interfaces create *immobile* films that reduce drainage through surface stress dissipation, while surface inviscid surfaces create *mobile* interfaces and create surface-tension induced Marangoni flows that counter the bulk-flow direction.

<https://doi.org/10.1371/journal.pone.0175753.g008>

(Alabaster, AL) in 25 mg mL^{-1} glass vials. We diluted it to a concentration of 1 mg mL^{-1} in chloroform (Sigma-Aldrich, St. Louis, MO) and stock solutions were kept in freezer until use. To achieve a desired surface pressure, we spread DPPC at the interface, and compressed using a teflon barrier. SDS (Sigma-Aldrich, St. Louis, MO) solutions were prepared using phosphate buffer saline (PBS, 50 mM, pH 7.0; Gibco) to a desired concentrations of 0.28 mM and 10 mM. These particular concentrations were chosen to investigate the effect of micelles on the stability of draining films. It is important to note that the critical micelle concentration (cmc) of SDS in buffered solution is 2 mM [33].

Experimental setup

A photograph and a schematic of the apparatus used to characterize the drainage of thin films are shown in Fig 1, which is similar to the drainage apparatus used previously for study of lung surfactants [7], and a slight modification for the study of tear film [6]. Unlike the titanium dome with contact lens, the solid curved glass dome (Newport KPX579, with a curvature of 19.9 mm) is mounted on a pedestal. It is initially submerged in the solution filled Teflon mini-Langmuir trough that is fixed onto a stationary support structure. The trough enables the spreading of insoluble surfactant (DPPC) on aqueous subphase at a controlled surface pressure. Having a controlled surface pressure is important as the interfacial shear rheology is a strong function of surface pressure. It is also important to mention that the reported experiments were all conducted at room temperature (23°C), and since the duration of the experiments $< 10 \text{ s}$, evaporative stresses are negligible (S1 & S2 Figs). In the case of DPPC, the surface pressure is continuously monitored using a paper Wilhelmy balance connected to a surface pressure sensor (KSV NIMA Ltd., Helsinki, Finland), and only a small deviation of $\pm 0.3 \text{ mN m}^{-1}$ is observed. However, for SDS, the glass dome is initially submerged in SDS-filled trough, and the adsorption equilibrium is awaited. Once the desired surface pressure is reached in both cases, the dome is elevated using a motorized stage through the interface, and captures a thin liquid film. The thickness of this film is measured using a high speed white light interferometer (F70, Filmetrics, USA) combined with a halogen light (Fiber-Lite PL-800).

The following protocol was followed while conducting the experiment. The glass dome is initially positioned approximately $130 \mu\text{m}$ below the interface. The dome is then raised 2.5 mm at various speed, V_e , ranging from $1\text{--}10 \text{ mm s}^{-1}$ and the thickness of the film, h , is captured by the interferometer. For every dataset, the height versus time data was fitted with the theoretical model to attain a characteristic value of the fitting parameter α .

Visualization of surface flows

To assess and visualize the interfacial and Marangoni stress-induced flows, the drainage setup was slightly modified. The elevating glass dome was replaced by an elevating air bubble (1.1 mm , dia) as shown in Fig 5. The air bubble, generated at the tip of the glass capillary (Drummond Micropipette, Fisher Scientific Inc., MA, USA) approaches an air-liquid interface in the presence of surfactants. The use of an air bubble instead of a glass dome provides a better index of refraction contrast. The air bubble is initially positioned approximately $100 \mu\text{m}$ below the interface. The air bubble is then elevated at the speed of 0.3 mm s^{-1} by a vertical distance of 0.6 mm for DPPC and 1 mm for SDS. These particular vertical distances are chosen to ensure that only a fraction of the bubble cap is exposed at the interface. Under white light illumination ($420\text{--}780 \text{ nm}$), the color interference patterns of these thin curved films ($< 1 \mu\text{m}$) are captured using a color CCD camera.

Supporting information

S1 Fig. SDS time scales. (A) Adsorption time scales for SDS at 0.13 cmc and 5 cmc. (B) Duration of drainage for SDS films at above and below cmc. (C & D) Representative drainage results of below and above cmc of SDS at 1 mm s^{-1} , with b corresponding to our fitting parameter α . (TIFF)

S2 Fig. DPPC drainage duration. Raw-data showing duration of drainage (in seconds) for DPPC films at different surface pressures and elevation velocities. (TIFF)

S1 Video. DPPC low pressure surface flows. Surface visualization flows for DPPC at 5 mN m^{-1} . (MOV)

S2 Video. DPPC high pressure surface flows. Surface visualizations flows for DPPC at $>25 \text{ mN m}^{-1}$. (MOV)

S3 Video. SDS above cmc surface flows. Surface visualization flows for SDS (above CMC). (MOV)

S4 Video. SDS below cmc surface flows. Surface visualization flows for SDS (below CMC). (MOV)

Acknowledgments

The authors would like to thank Daniele Tammaro and John Frostad for useful discussions. J. T. acknowledges a grant from UNED's Researchers Formation Program and partial support from MINECO (Grant FIS2013-47350-C5-5-R).

Author Contributions

Conceptualization: MSB GGF.

Formal analysis: MSB CC.

Investigation: CC MAV JT.

Methodology: MSB CC MAV JT.

Project administration: MSB GGF.

Resources: GGF.

Supervision: MSB GGF.

Validation: MSB.

Visualization: MSB CC.

Writing – original draft: MSB CC.

Writing – review & editing: MSB CC GGF.

References

1. Behera MR, Varade SR, Ghosh P, Paul P, Negi AS. Foaming in micellar solutions: Effects of surfactant, salt, and oil concentrations. *Industrial and engineering chemistry research*. 2014; 53(48):18497–18507. <https://doi.org/10.1021/ie503591v>

2. Debrégeas G, De Gennes PG, Brochard-Wyart F. The life and death of 'bare' viscous bubbles. *Science*. 1998; 279(5357):1704–1707. <https://doi.org/10.1126/science.279.5357.1704>
3. Feng J, Roché M, Vigolo D, Arnaudov LN, Stoyanov SD, Gurkov TD, et al. Nanoemulsions obtained via bubble-bursting at a compound interface. *Nature Physics*. 2014; 10(8):606–612. <https://doi.org/10.1038/nphys3003>
4. Bird JC, de Ruiter R, Courbin L, Stone HA. Daughter bubble cascades produced by folding of ruptured thin films. *Nature*. 2010; 465(7299):759–762. <https://doi.org/10.1038/nature09069> PMID: 20535206
5. Cooper A, Kennedy MW. Biofoams and natural protein surfactants. *Biophysical Chemistry*. 2010; 151(3):96–104. <https://doi.org/10.1016/j.bpc.2010.06.006> PMID: 20615601
6. Bhamla MS, Giacomini CE, Balemans C, Fuller GG. Influence of interfacial rheology on drainage from curved surfaces. *Soft Matter*. 2014; 10(36):6917–6925. <https://doi.org/10.1039/C3SM52934G> PMID: 25140576
7. Hermans E, Bhamla MS, Kao P, Fuller GG, Vermant J. Lung surfactants and different contributions to thin film stability. *Soft Matter*. 2015; 11(41):8048–8057. <https://doi.org/10.1039/C5SM01603G> PMID: 26307946
8. Radoev BP, Scheludko AD, Manev ED. Critical thickness of thin liquid films: Theory and experiment. *Journal of Colloid and Interface Science*. 1983; 95(1):254–265. [https://doi.org/10.1016/0021-9797\(83\)90094-2](https://doi.org/10.1016/0021-9797(83)90094-2)
9. Nikolov AD, Wasan DT, Denkov ND, Kralchevsky PA, Ivanov IB. Drainage of foam films in the presence of nonionic micelles. In: *Surfactants and Macromolecules: Self-Assembly at Interfaces and in Bulk*. Darmstadt: Steinkopff; 1990. p. 87–98.
10. Mysels KJ, Cox MC. An experimental test of Frankel's law of film thickness. *Journal of Colloid Science*. 1962; 17(2):136–145. [https://doi.org/10.1016/0095-8522\(62\)90004-1](https://doi.org/10.1016/0095-8522(62)90004-1)
11. Lyklema J, Scholten PC, Mysels KJ. Flow in Thin Liquid Films. *Journal of Physical Chemistry*. 1965; 69(1):116–123. <https://doi.org/10.1021/j100885a018>
12. Shen AQ, Gleason B, McKinley GH, Stone HA. Fiber coating with surfactant solutions. *Physics of Fluids*. 2002; 14(11):4055. <https://doi.org/10.1063/1.1512287>
13. Naire S, Braun R, Snow S. An Insoluble Surfactant Model for a Vertical Draining Free Film. *Journal of Colloid and Interface Science*. 2000; 230(1):91–106. <https://doi.org/10.1006/jcis.2000.7081> PMID: 10998292
14. Naire S, Braun RJ, Snow SA. An insoluble surfactant model for a vertical draining free film with variable surface viscosity. *Physics of Fluids*. 2001; 13(9):2492. <https://doi.org/10.1063/1.1388540>
15. Naire S, Braun RJ, Snow SA. A 2+1 dimensional insoluble surfactant model for a vertical draining free film. *Journal of Computational and Applied Mathematics*. 2004; 166(2):385–410. <https://doi.org/10.1016/j.cam.2003.08.039>
16. Joye JL, Hirasaki GJ, Miller CA. Asymmetric Drainage in Foam Films. *Langmuir*. 1994; 10(9):3174–3179. <https://doi.org/10.1021/la00021a046>
17. Joye JL, Hirasaki GJ, Miller CA. Numerical Simulation of Instability Causing Asymmetric Drainage in Foam Films. *Journal of Colloid and Interface Science*. 1996; 177(2):542–552. <https://doi.org/10.1006/jcis.1996.0068>
18. Choi SQ, Steltenkamp S, Zasadzinski JA, Squires TM. Active microrheology and simultaneous visualization of sheared phospholipid monolayers. *Nature communications*. 2011; 2:312. <https://doi.org/10.1038/ncomms1321> PMID: 21587229
19. Hermans E, Vermant J. Interfacial shear rheology of DPPC under physiologically relevant conditions. *Soft Matter*. 2014; 10(1):175–186. <https://doi.org/10.1039/C3SM52091A> PMID: 24651838
20. Zell ZA, Nowbahar A, Mansard V, Leal LG, Deshmukh SS, Mecca JM, et al. Surface shear inviscidity of soluble surfactants. *Proceedings of the National Academy of Sciences*. 2014; 111(10):3677–3682. <https://doi.org/10.1073/pnas.1315991111>
21. Bhamla MS, Balemans C, Fuller GG. Dewetting and deposition of thin films with insoluble surfactants from curved silicone hydrogel substrates. *Journal of Colloid and Interface Science*. 2015; 449:428–435. <https://doi.org/10.1016/j.jcis.2015.01.002> PMID: 25628055
22. Anton N, Pierrat P, Lebeau L, Vandamme TF, Bouriat P. A study of insoluble monolayers by deposition at a bubble interface. *Soft Matter*. 2013; 9(42):10081–10091. <https://doi.org/10.1039/c3sm51688a>
23. Kim K, Choi SQ, Zell ZA, Squires TM, Zasadzinski JA. Effect of cholesterol nanodomains on monolayer morphology and dynamics. *Proceedings of the National Academy of Sciences of the United States of America*. 2013; 110(33):E3054–60. <https://doi.org/10.1073/pnas.1303304110> PMID: 23901107
24. Leal LG. *Advanced transport phenomena: fluid mechanics and convective transport processes*. Fluid Mechanics and Convective Transport Processes. Cambridge: Cambridge; New York: Cambridge University Press; 2007.

25. Stebe KJ, Lin SY, Maldarelli C. Remobilizing surfactant retarded fluid particle interfaces. I. Stress-free conditions at the interfaces of micellar solutions of surfactants with fast sorption kinetics. *Physics of Fluids A: Fluid Dynamics* (1989–1993). 1991; 3(1):3–20. <https://doi.org/10.1063/1.857862>
26. Patist A, Oh SG, Leung R, Shah DO. Kinetics of micellization: its significance to technological processes. *Colloids and Surfaces A: Physicochemical and Engineering Aspects*. 2001; 176(1):3–16. [https://doi.org/10.1016/S0927-7757\(00\)00610-5](https://doi.org/10.1016/S0927-7757(00)00610-5)
27. Nierstrasz VA, Frens G. Marangoni Flow Driven Instabilities and Marginal Regeneration. *Journal of Colloid and Interface Science*. 2001; 234(1):162–167. <https://doi.org/10.1006/jcis.2000.7290> PMID: 11161503
28. Nierstrasz VA, Frens G. Marginal Regeneration and the Marangoni Effect. *Journal of Colloid and Interface Science*. 1999; 215(1):28–35. <https://doi.org/10.1006/jcis.1999.6226> PMID: 10362469
29. Nierstrasz VA, Frens G. Marginal Regeneration in Thin Vertical Liquid Films. *Journal of Colloid and Interface Science*. 1998; 207(2):209–217. <https://doi.org/10.1006/jcis.1998.5646> PMID: 9792764
30. Stein HN. On marginal regeneration. *Advances in Colloid and Interface Science*. 1991; 34:175–190. [https://doi.org/10.1016/0001-8686\(91\)80050-T](https://doi.org/10.1016/0001-8686(91)80050-T)
31. Hudaes JBM, Stein HN. Marginal regeneration of a mobile vertical free liquid film. *Journal of Colloid and Interface Science*. 1990; 138(2):354–364. [https://doi.org/10.1016/0021-9797\(90\)90218-D](https://doi.org/10.1016/0021-9797(90)90218-D)
32. Ramdane OO, Quéré D. Thickening factor in Marangoni coating. *Langmuir*. 1997; 13(11):2911–2916. <https://doi.org/10.1021/la961020a>
33. Sureshbabu N, Kirubakaran R, Jayakumar R. Surfactant-induced conformational transition of amyloid β -peptide. *European Biophysics Journal*. 2008; 38(4):355–367. <https://doi.org/10.1007/s00249-008-0379-8> PMID: 19005650